Astronomy & Astrophysics manuscript no. main
March 28, 2023

Calculating the CMB power spectrum (or a more spicy title)

Nanna Bryne[1,2]

[1] Institute of Theoretical Astrophysics (ITA), University of Oslo, P.O. Box 1029 Blindern, N-0315 Oslo, Norway
[2] Center for Computing in Science Education (CCSE), Dept. of Physics, University of Oslo, P.O. Box 1048 Blindern, N-0316 Oslo, Norway
e-mail: nanna.bryne@fys.uio.no

March 28, 2023

ABSTRACT

Context. ...
Aims. ...
Methods. ...
Results. ...
Conclusions. ...

Key words. cosmic microwave background - large-scale structure of universe

1. Introduction

The overall purpose of this project is to produce a program that calculates the Cosmic Microwave Background (CMB) power spectrum and predict the CMB and matter fluctuations through it. We want to achieve this starting from first principles. A large part of this paper follows Callin (2006).

We consider the concordance model of cosmology model that a Euclidean universe currently dominated by non-baryonic cold dark matter (CDM) and a cosmological constant (Λ), namely the (flat) ΛCDM model. The cosmological constant Λ is used as a moniker for dark energy (DE). (Dodelson & Schmidt 2021)

Complementary material to this paper can be found in our Github repository at `https://github.com/nannabryne/AST5220`.

2. Background cosmology

The first ingredient in the aforementioned program is a numerical framework describing the (unperturbed) background geometry. Said geometry is determined by the Friedmann-Robertson-Walker (FRW) metric and, as a starting point, a flatness assumption. However, we keep the variables associated with the curvature, the reasoning behind which will become clear shortly.

We want to describe the evolution of the Hubble parameter, conformal time and distance measures, all as functions of the logarithmic scale factor, $x = \ln a$, working as the main time variable in this paper. This is to be done with the use of the fiducial parameters ("fiducials") from Planck Collaboration et al. (2021).

The implementation of these functions results in a cosmological model that we can play around with. Our next task is to use observational data from Betoule et al. (2014) to tweak the default cosmological parameters and evaluate their credibility, curvature being one of the parameters. In particular, we will use a Monte Carlo Markov Chain (MCMC) with Metropolis algorithm to explore the parameter space of our model to infer their properties and compare them with observations from supernovae.

MCMC is a popular statistical technique used in various fields besides cosmology. The Metropolis algorithm, a simple and widely used MCMC method, generates a Markov chain of samples in a data set that converge to the target distribution by iteratively accepting or rejecting proposed moves in parameter space based on a set of acceptance criteria.

2.1. Theory

The FRW line element in flat space is given by

$$\begin{aligned} ds^2 &= -c^2\,\mathrm{d}t^2 + a^2(t)\delta_{ij}\,\mathrm{d}x^i\,\mathrm{d}x^j \qquad \mid \mathrm{d}\eta \equiv c\,\mathrm{d}t\,a^{-1}(t) \\ &= a^2(t)\left(-\mathrm{d}\eta^2 + \delta_{ij}\,\mathrm{d}x^i\,\mathrm{d}x^j\right). \end{aligned} \tag{1}$$

Before we proceed, we substitute $a \to \mathrm{e}^x$ (recall: $x = \ln a$). The cosmic time t and Hubble parameter H ($= \mathrm{d}x/\mathrm{d}t$) will be replaced by the conformal time η ($\mathrm{d}\eta = c\mathrm{e}^{-x}\,\mathrm{d}t$) and conformal Hubble parameter $\mathcal{H} \equiv aH$ ($= c\,\mathrm{d}x/\mathrm{d}\eta$). We write the Friedmann equations in terms of our preferred variables, which for the first one becomes

$$\mathcal{H}(x) = H_0\sqrt{\Omega_{\mathrm{m}0}\mathrm{e}^{-x} + \Omega_{\mathrm{r}0}\mathrm{e}^{-2x} + \Omega_{\mathrm{K}0} + \Omega_{\Lambda 0}\mathrm{e}^{2x}}, \tag{2}$$

the components of which are to be discussed shortly. The operator

$$\frac{\mathrm{d}}{\mathrm{d}x} = \frac{c}{\mathcal{H}}\frac{\mathrm{d}}{\mathrm{d}\eta} = \frac{1}{H}\frac{\mathrm{d}}{\mathrm{d}t} \tag{3}$$

proves useful, giving both the ordinary differential equation (ODE) for $\eta(x)$ and $t(x)$,

$$\frac{\mathrm{d}\eta}{\mathrm{d}x} = \frac{c}{\mathcal{H}(x)}\,; \qquad \eta(x_{\mathrm{init}}) = \eta_{\mathrm{init}}, \tag{4a}$$

$$\frac{\mathrm{d}t}{\mathrm{d}x} = \frac{1}{H} = \frac{\mathrm{e}^x}{\mathcal{H}(x)}\,; \qquad t(x_{\mathrm{init}}) = t_{\mathrm{init}}, \tag{4b}$$

where, in theory, $x_{\rm init} \to -\infty$ and the initial conditions $t_{\rm init}$, $\eta_{\rm init} \to 0$. However, we can solve Eq. (4) analytically in the very early universe and in Sect. 2.1.2 we present these expressions (Eq. (13)).

The conformal time is a useful time measure for large-scale cosmology as it takes into account the expansion of the universe. $\eta(x)$ measures the comoving distance that non-interacting photons could have travelled since the beginning where $x = -\infty$ ($t = 0$). Thus, the conformal time represents an upper limit to how far information could possibly travel. We say that regions that are separated by distances larger than this quantity are causally *dis*connected. For this reason, some books refer to $\eta(x)$ as the comoving horizon. (Dodelson & Schmidt 2021)

Finally, the cosmological redshift $z = \mathrm{e}^{-x} - 1$ will be used as an auxiliary time variable.

2.1.1. Density parameters

We assume the constituents of the universe to be cold dark matter (CDM (c)), baryons (b), photons (γ), neutrinos (ν) and a cosmological constant (Λ). We may regard the curvature (K) as a constituent as well. The evolution of the density parameter Ω_s associated with cosmological component $s \in \{\mathrm{c}, \mathrm{b}, \gamma, \nu, \Lambda, \mathrm{K}\}$ can be described in terms of our preferred variables as

$$\Omega_s(x) = \frac{\Omega_{s0}}{\mathrm{e}^{(1+3w_s)x}\mathcal{H}^2(x)/H_0^2}\,; \quad \Omega_{s0} \equiv \Omega_s(x = x_0), \tag{5}$$

where H_0 is the Hubble constant, $x_0 = \ln a_0 = 0$ means *today* and the *equation of state* parameter w_s is a constant intrinsic to the species s. As a notational relief, we introduce the parameters associated with total matter (m) and relativistic particles (r) such that $w_{\rm m} = 0$, $w_{\rm r} = 1/3$, $w_\Lambda = -1$ and $w_{\rm K} = -1/3$, and

$$\Omega_{\rm m} = \Omega_{\rm c} + \Omega_{\rm b} \quad \text{and} \quad \Omega_{\rm r} = \Omega_\gamma + \Omega_\nu. \tag{6}$$

Eq. (5) requires the current values of the density parameters. The observed CMB temperature today $T_{\rm CMB0}$ gives today's photon density

$$\Omega_{\gamma 0} = 2\frac{\pi^2}{30}\frac{(k_{\rm B}T_{\rm CMB0})^4}{\hbar^3 c^5}\frac{8\pi G}{3H_0^2}, \tag{7}$$

and followingly the neutrino density today

$$\Omega_{\nu 0} = N_{\rm eff}\cdot\frac{7}{8}\left(\frac{4}{11}\right)^{4/3}\Omega_{\gamma 0}, \tag{8}$$

$N_{\rm eff}$ being the effective number of massless neutrinos. From the Friedmann equations, the total density adds up to one, so we can determine the cosmological constant through $\Omega_{\Lambda 0} = 1 - \sum_s \Omega_{s0}$. Together with current values for the remaining densities, we have the evolution of all the considered constituents' densities as functions of x. This allows us to pinpoint the time when the total matter and radiation densities are equal—the "radiation-matter equality"—as $\Omega_{\rm m}(x = x_{\rm eq}) = \Omega_{\rm r}(x = x_{\rm eq})$. Further, we find the time at which the universe becomes dominated by the cosmological constant as $\Omega_\Lambda(x = x_\Lambda) = \Omega_{\rm m}(x = x_\Lambda)$. We obtain the analytical expressions

$$x_{\rm eq} = \ln\frac{\Omega_{\rm r0}}{\Omega_{\rm m0}} \quad \text{and} \quad x_\Lambda = \frac{1}{3}\ln\frac{\Omega_{\rm m0}}{\Omega_{\Lambda 0}}. \tag{9}$$

2.1.2. Cosmic expansion

To study the geometry of the universe, we want to know when the expansion started, i.e. when the universe started accelerating: $\mathrm{d}^2a/\mathrm{d}t^2$. It is trivial to show that this condition is equivalent to requiring $\mathrm{d}\mathcal{H}/\mathrm{d}x\,|_{x=x_{\rm acc}} = 0$. In App. A we present analytical expressions for the derivatives of $\mathcal{H}(x)$ in x. Studying these expressions, we expect to see that the start of acceleration and time of matter-dark energy transition are close to each other ($x_{\rm acc} \sim x_\Lambda$). Using Eq. (A.3) and arguing that the radiation term vanishes, we get

$$x_{\rm acc} = \frac{1}{3}\ln\frac{\Omega_{\rm m0}}{2\Omega_{\Lambda 0}} = x_\Lambda - \frac{1}{3}\ln 2 \tag{10}$$

for the acceleration onset.

The first Friedmann equation can be written in the general form

$$\mathcal{H}(x) = H_0\sqrt{\sum_s \Omega_{s0}\mathrm{e}^{-(1+3w_s)x}}, \tag{11}$$

where sum over s is a sum over the constituents in the universe ($s \in \{\mathrm{m}, \mathrm{r}, \Lambda, \mathrm{K}\}$). In an era where e.g. radiation dominates heavily ($\Omega_{\rm r}(x) \to 1$), the parameter resembles that of a universe with $\Omega_{\rm r0} = 1$ and so $\mathcal{H}(x) \simeq H_0\sqrt{\Omega_{\rm r0}}\mathrm{e}^{-2x}$. In more general terms, the conformal Hubble factor during an era dominated by a collection of particles with the same equation of state—a species s—is approximated

$$\mathcal{H}(x) \simeq H_0\sqrt{\Omega_{s0}}\mathrm{e}^{-\frac{x}{2}(1+3w_s)}. \tag{12}$$

If for said species we have $\Omega_s(x) \simeq 1$, we get $\Omega_{s'}(x) \ll 1$ for the others, and we expect this to be very close to equality.

In the very early universe, only relativistic particles were present. Conveniently, this gives nice expressions for the initial conditions for Eq. (4):

$$\eta_{\rm init} = \int_{-\infty}^{x_{\rm init}}\mathrm{d}x\,\frac{c\mathrm{e}^x}{H_0\sqrt{\Omega_{\rm r0}}} = \frac{c}{\mathcal{H}(x_{\rm init})} \tag{13a}$$

$$t_{\rm init} = \int_{-\infty}^{x_{\rm init}}\mathrm{d}x\,\frac{\mathrm{e}^x\mathrm{e}^x}{H_0\sqrt{\Omega_{\rm r0}}} = \frac{\mathrm{e}^{x_{\rm init}}}{2\mathcal{H}(x_{\rm init})} \tag{13b}$$

Choosing such initial conditions, it is important to make sure $x_{\rm init} \ll x_{\rm eq}$ so that the approximation $\mathcal{H}(x) \simeq H_0\sqrt{\Omega_{\rm r0}}\mathrm{e}^{-x}$ is viable.

2.1.3. Distance measures

Say we want to allow for the possibility of an open ($k = -1$) or closed ($k = +1$) universe, as opposed to the initial flatness ($k = 0$) assumption. In spherical coordinates, the FRW line element (Eq. (1)) is

$$ds^2 = \mathrm{e}^{2x}\left(-\mathrm{d}\eta^2 + \frac{\mathrm{d}r^2}{1-kr^2} + r^2\,\mathrm{d}\theta^2 + r^2\sin^2\theta\,\mathrm{d}\phi^2\right), \tag{14}$$

and $k = -\Omega_{\rm K0}H_0^2/c^2$. Consider a radially moving ($\mathrm{d}r < 0$; $\mathrm{d}\theta^2 = \mathrm{d}\phi^2 = 0$) photon ($ds^2 = 0$) travelling from a distance r at conformal time η to reach Earth ($r = 0$) today ($\eta = \eta_0$). Eq. (14) gives

$$\int_r^0 \mathrm{d}r'\,\frac{-1}{\sqrt{1-kr'^2}} = \int_\eta^{\eta_0}\mathrm{d}\eta' \tag{15}$$

of which the right-hand side is the comoving distance $\chi = \eta_0 - \eta$. We evaluate the left integral in Eq. (15) and find

$$r(\chi) = \begin{cases} \chi \cdot \frac{\sin\left(\sqrt{|\Omega_{K0}|} H_0 \chi / c\right)}{\sqrt{|\Omega_{K0}|} H_0 \chi / c} & \Omega_{K0} < 0 \\ \chi & \Omega_{K0} = 0 \\ \chi \cdot \frac{\sinh\left(\sqrt{|\Omega_{K0}|} H_0 \chi / c\right)}{\sqrt{|\Omega_{K0}|} H_0 \chi / c} & \Omega_{K0} > 0 \end{cases}. \tag{16}$$

The angular diameter distance of an object of physical size D and angular size θ is $d_A = D/\theta$. From Eq. (14) we get $\mathrm{d}D = re^x \,\mathrm{d}\theta$ and so

$$d_A(x) = re^x. \tag{17}$$

The luminosity distance is $d_L = d_A e^{-2x}$, giving

$$d_L(x) = re^{-x}. \tag{18}$$

2.2. Implementation details

The code we wrote included a class in C++ representing the background. In particular, this class requires current values of the density parameters Ω_{b0}, Ω_{c0} and Ω_{K0}, the CMB temperature today (T_{CMB0}) and the effective neutrino number (N_{eff}). In addition, the class needs the "little" Hubble constant $h = H_0$ [100 km s^{-1} Mpc^{-1}]. The remaining density parameters are computed as elaborated in Sect. 2.1. Amongst the class methods are functions for computing $\mathcal{H}(x)$, $\mathrm{d}\mathcal{H}(x)/\mathrm{d}x$, $\mathrm{d}^2\mathcal{H}(x)/\mathrm{d}x^2$ and $\Omega_{s0}(x)$ for some x, as well as code that solves the ODEs for $\eta(x)$ and $t(x)$. Another vital method is the one that yields the luminosity distance $d_L(x)$ for some x.

The specifics of our model was found from fits from Planck Collaboration et al. (2021):

$$\begin{aligned} \text{Hubble constant:} \quad & h = 0.67 \\ \text{CMB temperature:} \quad & T_{CMB0} = 2.7255 \text{ K} \\ \text{effective Neutrino number:} \quad & N_{eff} = 3.046 \\ \text{baryon density:} \quad & \Omega_{b0} = 0.05 \\ \text{CDM density:} \quad & \Omega_{c0} = 0.267 \\ \text{curvature density:} \quad & \Omega_{K0} = 0 \end{aligned} \tag{19}$$

This gave the following derived parameters:

$$\begin{aligned} \text{photon density:} \quad & \Omega_{\gamma 0} = 5.51 \times 10^{-5} \\ \text{neutrino density:} \quad & \Omega_{\nu 0} = 3.81 \times 10^{-5} \\ \text{DE density:} \quad & \Omega_{\Lambda 0} = 0.683 \end{aligned} \tag{20}$$

We evaluated the various quantities over $x \in [-20, 5]$, the same interval for which we numerically solved the ODEs for $\eta(x)$ and $t(x)$ in Eq. (4), setting $x_{init} = -20$ in Eq. (13). For integration method, we used Runge-Kutta 4 (RK4) with 1×10^5 steps.

After controlling our model by comparing numerical results to analytical expressions in limit cases, we turned our attention to the observational data from Betoule et al. (2014). The data set is constructed as follows: for each redshift z_i, there is an observed luminosity distance $d_L^{obs}(z_i)$ and an associated error $\sigma_{err}(z_i)$.

Subsequently, we wrote a script to perform an MCMC for the parameters h, Ω_{m0} and Ω_{K0}. Running said script, we compared the computed luminosity distance $d_L(z)$ from a cosmological model (an instance of the class) to the observed luminosity distance $d_L^{obs}(z)$ through the χ^2-function,

$$\chi^2(h, \Omega_{m0}, \Omega_{K0}) = \sum_{i=1}^{N} \frac{\left(d_L(z_i; h, \Omega_{m0}, \Omega_{K0}) - d_L^{obs}(z_i)\right)^2}{\sigma_{err}^2(z_i)}, \tag{21}$$

where $N = 31$ is the number of data points. The best-fit model was considered as the one for which $\chi^2 = \chi^2_{min}$, the lowest number found by the algorithm. A good fit is considered to have $\chi^2/N \sim 1$.

The MCMC analysis was characterised by a maximum of 10 000 iterations and the following limitations:

$$\begin{aligned} 0.5 \leq \quad & h \quad \leq 1.5 \\ 0.0 \leq \quad & \Omega_{m0} \quad \leq 1.0 \\ -1.0 \leq \quad & \Omega_{K0} \quad \leq 1.0 \end{aligned} \tag{22}$$

They were initialised by sample from a uniform distribution in the respective range. Once the code was executed successfully, we discard the first 200 samples, expecting this to be the approximate burn-in period for of the Metropolis MCMC.

2.3. Results

The familiar plot of the density parameters as functions of the logarithmic scale factor is presented in Fig. 1 together with markings of important milestones in the history of the universe (see Tab. 1).

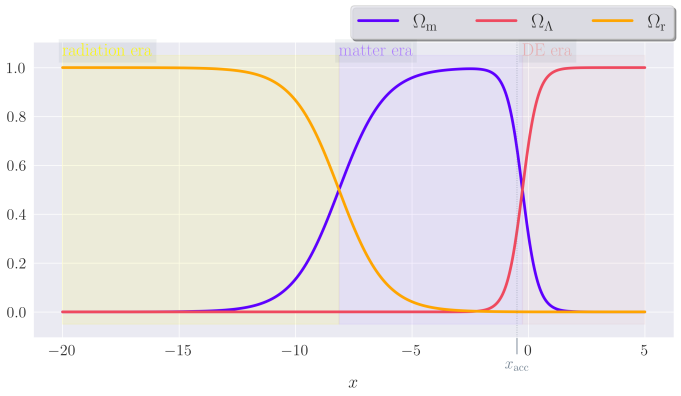

Fig. 1: The graphs show the evolution of the total matter density $\Omega_m(x)$, the total radiation density $\Omega_r(x)$ and the dark energy density $\Omega_\Lambda(x)$. The era of radiation ($x < x_{eq}$), matter ($x_{eq} < x < x_\Lambda$) and cosmological constant ($x > x_\Lambda$) domination are marked in yellow, purple and red, respectively.

The conformal Hubble factor and its derivatives are presented in Fig. 2 over-plotted with analytical predictions from the different eras (Tab. A.1). In the same figure you will find the product of the conformal time and Hubble factor.

The relationship between the cosmic and conformal time is demonstrated in Fig. 3, both quantities given in gigayears ("giga-annum" (Ga)).

We present the time of various milestones in the history of the universe, given this model, in Tab. 1 in our main time variable, redshift and cosmic time.

2.3.1. Supernova fitting

Before adjusting any parameters, we compared our initial model with the supernova data from Betoule et al. (2014). This by-eye comparison is found in Fig. 4. We demonstrated the model favoured by the data in the same plot.

The MCMC yielded $\chi^2_{min} = 29.28$ for the best-fit. We present confidence regions for Ω_{m0} and $\Omega_{\Lambda 0}$ in Fig. 5a at two levels; 68.4% and 95.5%. The distribution of the curvature parameter is

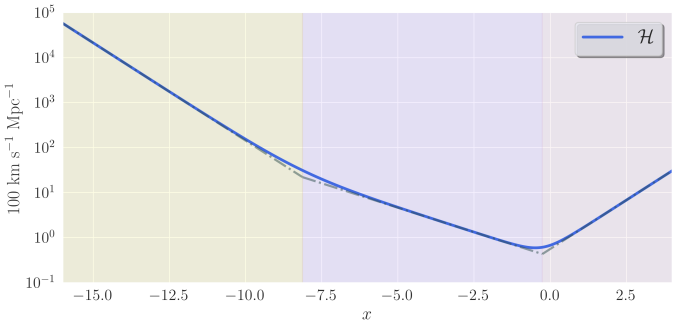

(a) The conformal Hubble factor $\mathcal{H}(x)$. The over-plotted dash-dotted line is the corresponding analytical estimate.

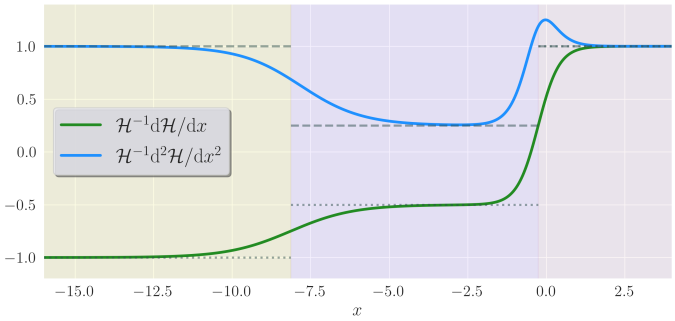

(b) The single and double derivative of the conformal Hubble factor, scaled with the factor itself, $\frac{1}{\mathcal{H}(x)}\frac{\mathrm{d}\mathcal{H}(x)}{\mathrm{d}x}$ and $\frac{1}{\mathcal{H}(x)}\frac{\mathrm{d}^2\mathcal{H}(x)}{\mathrm{d}x^2}$. The over-plotted dotted and dashed lines are the analytical estimates to the first and second derivative, respectively.

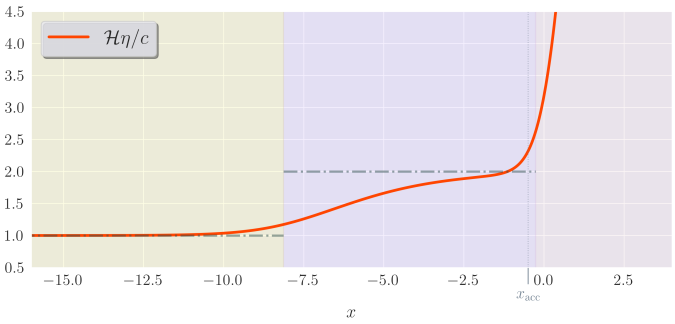

(c) The product of the conformal time and Hubble factor, divided by the speed of light, $\mathcal{H}(x)\frac{\eta(x)}{c}$. The solid graph blows up at late times. The over-plotted dash-dotted line is the corresponding analytical estimate (for single-substance universe).

Fig. 2: Plots demonstrating quantities related to the conformal Hubble parameter $\mathcal{H}(x)$ and the conformal time $\eta(x)$ as functions of logarithmic scale factor x. The dashed and/or dotted graphs are the predictions from Tab. A.1, i.e. what we expect in each era (indicated by different background colours, following Fig. 1) if all non-prevailing constituents can be neglected. The beginning of acceleration is indicated by a humble vertical line.

shown in Fig. 5b. As for the Hubble constant, the distribution is found in Fig. 5c. The distributions were fitted as normal distributions (demonstrated in Fig. 5) $\mathcal{N}(\mu, \sigma)$ with average μ (best-fit) and standard deviation σ (error). We got the following set of new best-fits:

$$\begin{aligned} h &= 0.70 \pm 0.01 \\ \Omega_{\mathrm{m0}} &= 0.26 \pm 0.10 \\ \Omega_{\Lambda 0} &= 0.66 \pm 0.16 \\ \Omega_{\mathrm{K0}} &= 0.08 \pm 0.25 \end{aligned} \tag{23}$$

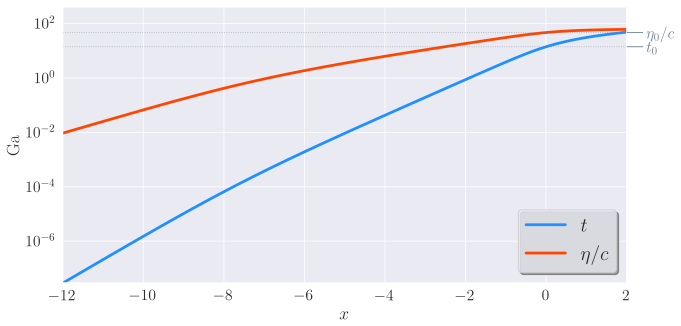

Fig. 3: Cosmic time $t(x)$ and conformal time per speed of light $\frac{\eta(x)}{c}$. Note the logarithmic y-axis.

Table 1: The values of the logarithmic scale factor x, the redshift z and the cosmic time t corresponding to four important milestones in the history of the universe.

	x	z	t
Rad.-matter equality	−8.132	3400	51.06 ka
Acceleration onset	−0.4869	0.6272	7.752 Ga
Matter-DE equality	−0.2558	0.2915	10.37 Ga
Today	−0.000	0.000	13.86 Ga
Conformal time today:		$\eta_0 = 46.32c$ Ga	

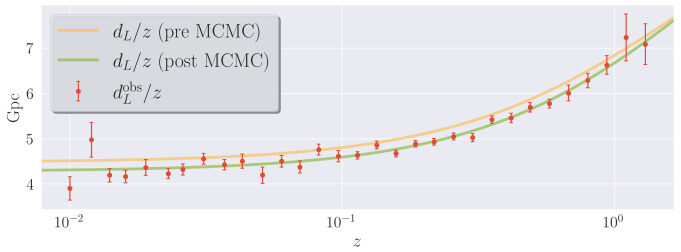

Fig. 4: The observed (dots) and computed (lines) luminosity distance per redshift $\frac{d_L^{\mathrm{obs}}(z)\pm\sigma_{\mathrm{err}}(z)}{z}$ and $\frac{d_L(z)}{z}$. The yellow line represents the fiducial model, whilst the green line is the revised model resulting from the MCMC.

2.4. Discussion

The graphs in Fig. 1 show that prior to $x \sim -15$, radiation was the prevailing constituent of matter and energy density in the universe, making $x_{\mathrm{init}} = -20$ in Sect. 2.1.2 a valid choice. The radiation era is followed by an era of matter domination before the universe enters its current epoch where dark energy is the preeminent contributor to the cosmic energy budget. The universe has not yet become overwhelmed by the dark energy, however, and we can see that we are currently in a transitional period between total matter domination and total DE domination. The graphs also show that this transitional period is much quicker than the previous one, and that just before matter-DE equality ($x = x_\Lambda$), the universe starts accelerating ($x = x_{\mathrm{acc}}$). We clearly see the relation between the dark energy suddenly becoming significant and the universe accelerating.

Our results, as shown in the graphs in Fig. 2, demonstrate that our code gives sensible results when modelling the evolution of the universe. The changes in the density parameters depicted in Fig. 1 offer insight into the transitional periods shown in Fig. 2a and Fig. 2b, which correspond to eras where no single

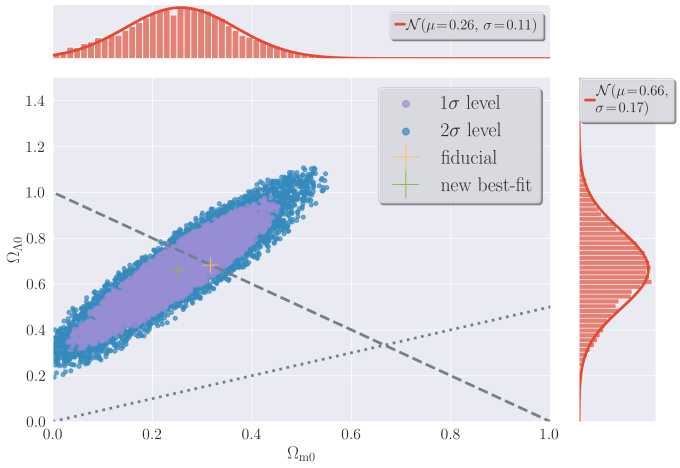

(a) The dots give constraints on the parameters that quantify the contribution of matter and cosmological constant to the cosmic energy budget today (Ω_{m0}, $\Omega_{\Lambda 0}$). The Planck parameters from Eq. (19) and Eq. (20) and the new best-fit parameters are indicated by crosses. The dashed grey line points to a flat universe; below/above this meaning an open/closed universe. The dotted grey line signifies zero acceleration; below/above indicating a decelerating/accelerating universe. The distributions of the accepted samples of Ω_{m0} and $\Omega_{\Lambda 0}$ are illustrated by the top and right panel, respectively.

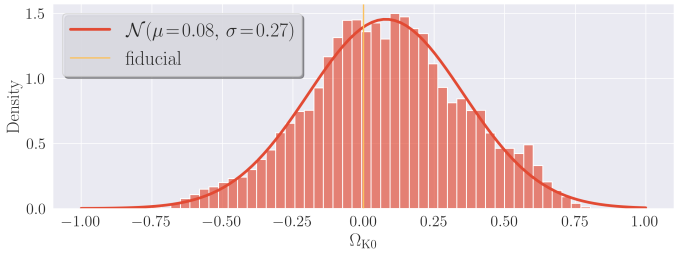

(b) Posterior distribution of parameter quantifying the contribution of curvature to the cosmic energy budget today.

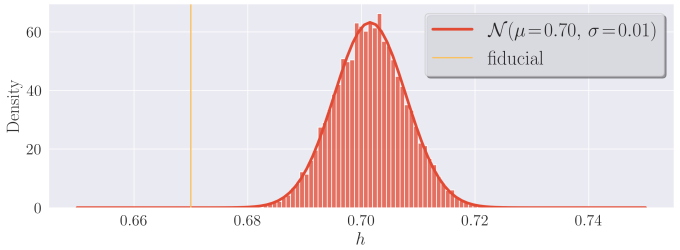

(c) Posterior distribution of the Hubble constant $h = H_0$ [100 km s^{-1} Mpc^{-1}].

Fig. 5: Results from the MCMC of 10 000 iterations. The histograms show the distributions of accepted samples and the curves are their PDFs.

substance dominates the universe. These findings are consistent with existing knowledge of the universe's history. Additionally, we observe that the conformal time cannot be accurately predicted in the same way for later eras, as demonstrated in Fig. 2c, exactly as expected (ref to some section).

In this model, the redshift of 3400 marks the epoch of radiation-matter equality, while the universe entered its current epoch approximately 3.5 gigayears ago as shown in Tab. 1. Additionally, our analysis reveals that the universe is estimated to be 13.9 gigayears old and has been accelerating for almost half of that time, starting at the age of 7.8 gigayears. These predictions differ slightly from those reported in the literature, such as an age of $t_0 = 13.78$ in Dodelson & Schmidt (2021). It is sufficient to argue that the main reason for such deviations is the (small) difference in choice of cosmological parameters. However, we would like to address the computational limitations: the choice of grid for x may introduce numerical vulnerabilities that propagate into other variables. For instance, as illustrated in Fig. 3, over 10 gigayears can pass between $x = -2$ and $x = 0$, even though we started integrating from $x = x_{\mathrm{init}} = -20$.

2.4.1. Supernova fitting

The comparison of our model's luminosity distance with observational data, as shown in Fig. 4 (ignoring the posterior green graph), suggests that our model could benefit from some adjustments. While the deviations are not too far off, it is clear that there is some room for improvement. However, it is important to note that the discrepancies may not be solely due to the three parameters we chose to study.

To further constrain our model, we performed an MCMC analysis and examined the resulting distributions of parameters. The scatter plot in Fig. 5a shows that our model requires an accelerating universe ($\mathrm{d}\mathcal{H}/\mathrm{d}x\,|_{x=x_0} > 0$) with a strictly positive cosmological constant ($\Omega_{\Lambda 0} > 0$). We notice that the Planck parameters lie within the 1σ region for (Ω_{m0}, $\Omega_{\Lambda 0}$), along the flat line. This is not the case for all the parameters, however.

Interestingly, the data clearly prefer a slightly higher value for the little Hubble parameter h than our fiducial value of 0.67, as shown in the narrow histogram in Fig. 5c. The PDFs of the density parameters Ω_{m0} and $\Omega_{\Lambda 0}$ are much broader, but the algorithm manages to narrow the possibilities down significantly.

One potential concern is the uncertainty in the curvature parameter Ω_{K0}, as shown in Fig. 5. The data seem to favour a negatively curved universe, but the allowed range is quite broad. This may indicate that our model needs further refinement to better account for the effects of curvature.

Overall, our primitive MCMC analysis provides valuable insights into the constraints on the parameters of our model and highlights areas where further improvements could be made. Other than with observational data from supernovae, there are several ways of constraining the cosmological parameters, such as measuring the CMB anisotropies. Planck Collaboration et al. (2021) provides a set of cosmological parameters that are significantly more solid, in the sense that their results are tested and compared thoroughly. This is why we proceed using the fiducials from Eq. (19) and Eq. (20).

3. Recombination history

After the Big Bang, the universe was in a state of high temperature and density, making it impossible for atoms to form. Instead, all matter existed as a highly ionised plasma. It was only when the universe began to expand and cool down that the conditions allowed for the combination of ions (protons) and electrons. This process resulted in the formation of atoms, primarily hydrogen and helium, during the "epoch of recombination" around 380 000 years after the Big Bang, when the temperature had dropped to around 3000 K. Prior to this, photons could not travel freely through the ionised plasma as they were scattered by free electrons. However, as free electrons combined with other baryons to form neutral atoms during recombination, the mean free path of the photons increased. The photons emitted during this period make up the CMB radiation.

We will in this section examine the free electron fraction and followingly the optical depth and visibility function. From these quantities, we find the time of recombination and surface of last scattering. In addition, we will compute the freeze-out free electron fraction and sound horizon at decoupling. Throughout this paper (section???) we ignore helium completely.

3.1. Theory

The process that keeping the photons (γ) coupled to electrons (e^-) in the early universe is called Thomson scattering and is the low-energy case of Compton scattering,

$$\gamma + e^- \leftrightarrows \gamma + e^-, \tag{24}$$

and considered to be the major source of opacity in the early universe. Going forward in time, the universe expanded and therefore cooled down, eventually to the temperature for which the combination of electrons and protons (p)—the formation of neutral hydrogen atoms (H)—was energetically favourable. As a result, the amount of free electrons (and protons), compared to the total number of baryons in the universe, rapidly decreased. As direct recombinations to the ground state are highly unlikely, a hydrogen atom generally arises from an electron in a high energy state that immediately decays to its ground state, emitting a photon in the process;

$$e^- + p \leftrightarrows \mathrm{H} + \gamma. \tag{25}$$

There are two main pathways from the first excited state ($n = 2$) to the ground state ($n = 1$):

- $2p \rightarrow 1s$: decay through the emission of a Lyman-α photon that is (almost exclusively) to be reabsorbed by another ground state hydrogen
- $2s \rightarrow 1s$: through the very slow process of 2-photon decay

These basic principles are amongst those that Jim Peebles and collaborators (see Peebles 1968) adopted in their model of non-equilibrium recombination history of hydrogen, described by the differential equation for the free electron abundance we call the *Peebles equation* (Eq. (33)). There are numerical difficulties when solving this equation for very early times—this is where we address the work of Meghnad Saha in 1920. The *Saha equation* (Eq. (29)) is applicable in systems of chemical equilibrium and relates the number densities of reactants to those of the products in a reaction (assuming the equilibrium density of each element is known). At early times, this is a viable assumption, and we can examine the abundance of free electrons in the universe at all times. (Peebles 1968; Ma & Bertschinger 1995; Callin 2006)

3.1.1. Optical depth and visibility

Photons travelling through a medium may be absorbed. The intensity of light emitted from a distance x is reduced by the factor $\mathrm{e}^{-\tau(x)}$ where $\tau(x)$ is the optical depth of the medium. An optically thin ($\tau \ll 1$) medium does little or no absorbing, whereas an optically thick ($\tau \gg 1$) substance does not let much, if any, light pass through. In cosmology, Thomson scattering is predominantly responsible for the absorption of photons universe. This, and the assumption that the universe is transparent today, gives us the ODE for $\tau(x)$,

$$\frac{\mathrm{d}\tau}{\mathrm{d}x} = -\frac{c n_e \sigma_\mathrm{T} \mathrm{e}^x}{\mathcal{H}(x)}, \tag{26}$$

with $\tau(0) = 0$, where σ_T is the Thomson scattering cross-section and n_e the electron density. A related quantity is the visibility function

$$\tilde{g}(x) = -\mathrm{e}^{-\tau(x)} \frac{\mathrm{d}\tau(x)}{\mathrm{d}x}, \tag{27}$$

a proper probability distribution obeying $\int_{-\infty}^{0} \mathrm{d}x\, \tilde{g}(x) = 1$. The probability it describes, is that of a CMB photon's last interaction with an electron to have happened at x. This function will have a peak at the point in time when the mean free path of the photons increased tremendously—at the last scattering surface—which happened immediately after the number of free electrons dropped dramatically—during recombination. In mathematical terms, this decoupling happened when $\tilde{g}(x_\mathrm{dec}) = \max \tilde{g}(x)$, or

$$\left.\frac{\mathrm{d}\tilde{g}(x)}{\mathrm{d}x}\right|_{x=x_\mathrm{dec}} = 0 \quad \Leftrightarrow \quad \left[\frac{\mathrm{d}^2\tau(x)}{\mathrm{d}x^2} = \left(\frac{\mathrm{d}\tau(x)}{\mathrm{d}x}\right)^2\right]_{x=x_\mathrm{dec}}. \tag{28}$$

The surface of last scattering can also be taken as the time when the universe is neither opaque nor transparent, i.e. the solution of $\tau(x = x_\mathrm{dec}) = 1$. We will use the former, but expect to see that $\tau(x_\mathrm{dec}) \simeq 1$ in any case.

We will take x_* to mean the logarithmic scale factor at the time of recombination, which will be so close to the last scattering surface that it will also refer to this point in time when the distinction is not important.

3.1.2. Hydrogen recombination

Before we can compute the optical depth, we need to know the electron number density, n_e, at all times. We define the free electron fraction $X_e \equiv n_e/n_\mathrm{b}$ where n_b is the total baryon number density. Before recombination, that is for $x \ll x_*$, all hydrogen is completely ionised, meaning that $X_e(x \ll x_*) \simeq 1$. We will let the time of recombination, x_*, be the solution to $X_e(x = x_*) = 0.1$. One should keep in mind that the number 0.1 is arbitrary and that this definition, as with x_dec, vary in the literature.

Consider the interaction that keeps electrons and protons in equilibrium with photons, i.e. Eq. (25). Letting n_s ($n_s^{(0)}$) denote the number density of a species/element s (in equilibrium), the corresponding equilibrium equation is

$$\frac{n_e n_p}{n_\mathrm{H}} = \frac{n_e^{(0)} n_p^{(0)}}{n_\mathrm{H}^{(0)}}, \tag{29}$$

known as the *Saha equation*. Likewise, letting m_s refer to the mass of s, we can take the number density of neutral hydrogen to be

$$n_\mathrm{H} = (1 - Y_P)\, n_\mathrm{b} \simeq (1 - Y_P)\, \frac{\Omega_{\mathrm{b}0}\rho_{\mathrm{cr}0}}{m_\mathrm{H}\mathrm{e}^{3x}}; \quad \rho_{\mathrm{cr}0} = \frac{3H_0^2}{8\pi G}, \tag{30}$$

where Y_P denotes the primordial helium mass fraction. We neglect helium s.t. $Y_P = 0$ and assume that all baryons are protons. Further, recognising the neutrality of the universe ensures $n_p = n_e$. Now, $n_\mathrm{b} = n_p + n_\mathrm{H}$ and

$$X_e = \frac{n_e}{n_e + n_\mathrm{H}} = \frac{n_p}{n_p + n_\mathrm{H}}. \tag{31}$$

Let $\Upsilon \equiv \epsilon_0/(k_\mathrm{B} T_\mathrm{b})$ for notational ease. Multiplying Eq. (29) by n_b^{-1} and inserting expressions for $n_s^{(0)}$, we obtain the more suggestive form of the Saha equation

$$\frac{X_e^2}{1 - X_e} = \frac{1}{n_\mathrm{b}} \left(\frac{m_e k_\mathrm{B} T_\mathrm{b}}{2\pi\hbar^2}\right)^{3/2} \mathrm{e}^{-\Upsilon}; \quad 0 < X_e \leq 1 \wedge X_e \sim 1. \tag{32}$$

The constraints on X_e are that it is a positive number that cannot exceed 1 and the observation that it has to be close to 1. The latter constraint is due to the equilibrium assumption from which the Saha equation is derived: as X_e falls the reaction rate for Eq. (25) falls and equilibrium is not guaranteed. To proceed,

we need to solve the Boltzmann equation. More precisely, Jim Peebles needed to solve the Boltzmann equation, whereas we will study the product; a first-order ODE the *Peebles equation*. Said equation reads

$$\frac{\mathrm{d}X_e}{\mathrm{d}x} = \frac{C_r(T_\mathrm{b})}{\mathcal{H}(x)\mathrm{e}^{-x}}\left[\beta(T_\mathrm{b})\left(1-X_e\right) - n_\mathrm{H}\alpha^{(2)}(T_\mathrm{b})X_e^2\right], \tag{33}$$

where the necessary mathematical expressions are the following:

$$C_r(T_\mathrm{b}) = \frac{\Lambda_{2s\to1s}+\Lambda_\alpha}{\Lambda_{2s\to1s}+\Lambda_\alpha+\beta^{(2)}(T_\mathrm{b})} \tag{34a}$$

$$\Lambda_{2s\to1s} = 8.227\ \mathrm{s}^{-1} \tag{34b}$$

$$\Lambda_\alpha = \frac{\mathcal{H}\mathrm{e}^{-x}}{(8\pi)^2 n_{1s}}\left(\frac{3\epsilon_0}{\hbar c}\right)^3 \tag{34c}$$

$$n_{1s} = (1-X_e)n_\mathrm{H} \tag{34d}$$

$$\beta^{(2)}(T_\mathrm{b}) = \beta(T_\mathrm{b})\mathrm{e}^{3/4\Upsilon} \tag{34e}$$

$$\beta(T_\mathrm{b}) = \alpha^{(2)}(T_\mathrm{b})\left(\frac{m_e k_\mathrm{B} T_\mathrm{b}}{2\pi\hbar^2}\right)^{3/2}\mathrm{e}^{-\Upsilon} \tag{34f}$$

$$\alpha^{(2)}(T_\mathrm{b}) = \frac{8c\sigma_\mathrm{T}}{\sqrt{3\pi}}\sqrt{\Upsilon}\phi_2(T_\mathrm{b}) \tag{34g}$$

$$\phi_2(T_\mathrm{b}) = 0.448\ln\Upsilon \tag{34h}$$

A detailed description of Eq. (34) is found in Peebles (1968). The decay rates Λ_α and $\Lambda_{2s\to1s}$ are the rates of the processes $2p\to1s$ and $2s\to1s$ mentioned in the beginning of Sect. 3.1, respectively. The reduction factor C_r is the ratio between the net decay rate and the combined decay and ionisation rates from the first excited level. Thus, $\beta^{(2)}$ represents the rate of reionisation (. . .)

The reduction factor is the probability that an atom in the first excited state reaches the ground state to one of the two pathways before being photoionised.

Necessary to describe components here??

(Dodelson & Schmidt 2021; Ma & Bertschinger 1995; Peebles 1968)

3.1.3. Sound horizon

The distance that a sound wave could propagate in the primordial plasma before photons decoupled is called "the sound horizon at decoupling", a quantity whose significance will become prominent in sections to come. We define the sound speed of a photon-baryon plasma as

$$c_s \equiv c\sqrt{\frac{1}{3(1+R)}}, \tag{35}$$

where the baryon-to-photon energy ratio is defined as

$$R \equiv \frac{\Omega_\mathrm{b}(x)}{\Omega_\gamma(x)} = \frac{3\Omega_{\mathrm{b}0}}{4\Omega_{\gamma0}}\mathrm{e}^x. \tag{36}$$

The comoving distance travelled by a sound wave—the sound horizon—at time x as the solution $r_s(x)$ to the ODE

$$\frac{\mathrm{d}r_s}{\mathrm{d}x} = \frac{c_s}{\mathcal{H}(x)}\,; \quad r_s(x_\mathrm{init}) = \frac{c_s(x_\mathrm{init})}{\mathcal{H}(x_\mathrm{init})}. \tag{37}$$

Evaluating $r_s(x=x_*)$ gives the sound horizon at decoupling (assuming $x_\mathrm{dec}\simeq x_*$). At this point, the plasma through which sound waves propagate is no longer present and the waves are frozen in.

3.2. Implementation details

We implemented a class in C++ that assumes a background, an object of the class from Sect. 2.2, and a primordial helium abundance Y_P. The code we wrote (1) calculated $X_e(x)$ (and $n_e(x)$) from the Saha and Peebles equations and (2) computed $\tau(x)$ as well as $\tilde{g}(x)$, $\mathrm{d}\tilde{g}(x)/\mathrm{d}x$ and $\mathrm{d}^2\tilde{g}(x)\big/\mathrm{d}x^2$ for a given array of x-values.

We ran an additional simulation where we assumed equilibrium all the way, that is we solved for $X_e(x)$ using only the Saha equation.

3.2.1. Electron fraction and number density

The computation of $X_e(x)$ was divided into two parts. We let $X_e(x) > 0.99$ signify the Saha regime for which we use the Saha approximation in Eq. (32). Numerically speaking, the solution to this equation,

$$X_e(x) = \frac{\mathfrak{U}}{2}\left(-1+\sqrt{1+4\mathfrak{U}^{-1}}\right)\,; \quad \mathfrak{U} = \frac{1}{n_\mathrm{b}}\left(\frac{m_e k_\mathrm{B} T_\mathrm{b}}{2\pi\hbar^2}\right)^{3/2}\mathrm{e}^{\Upsilon}, \tag{38}$$

blows up for large values of $\mathfrak{U}$. Analytically we have $X_e\to1$ as $\mathfrak{U}\to\infty$, so we circumvented the issue by letting $X_e = 1\ \forall\ \mathfrak{U} > 10^7$. Outside the Saha regime, we used the last value of $X_e(x)$ (≈ 0.99) as initial condition on the Peebles ODE (Eq. (33)) and solved this for the remaining values of x. Here as well, we needed to address numerical stability concerns. Specifically, $\beta^{(2)}$ in Eq. (34e) was set to zero when the exponent was too large; $\Upsilon > 200$, i.e. at later times when $T_\mathrm{b} < 0.005\epsilon_0/k_\mathrm{B} \sim 800$ K.

We solved for $8\times10^5+1$ equally spaced points $x\in[-12,0]$. The numerical integration was performed using RK4 and the number of steps left in the x-array at the end of the Saha regime.

3.2.2. Optical depth and visibility

We computed $\tau(x)$ by solving the simple ODE in Eq. (26) starting from $x=0$ where $\tau(0)=0$ and integrating backwards in time, using 8×10^5 steps along $x\in[0,-12]$ in the RK4 algorithm.

We used the analytical expressions in Eq. (26) and Eq. (27) for $\mathrm{d}\tau(x)/\mathrm{d}x$ and $\tilde{g}(x)$, respectively, and found $\mathrm{d}^2\tau(x)\big/\mathrm{d}x^2$, $\mathrm{d}\tilde{g}(x)/\mathrm{d}x$ and $\mathrm{d}^2\tilde{g}(x)\big/\mathrm{d}x^2$ numerically.

3.3. Results

The free electron fraction as computed from the Saha and Peebles equations in their respective regimes is plotted in Fig. 6. We added the result from using only the Saha equation. As elaborated in Sect. 3.2.2 we calculated the optical depth and visibility function and their derivatives. We present the optical depth and its derivatives in Fig. 7. The visibility function is demonstrated in Fig. 8, where we have included its derivatives scaled to be comparable to the original function.

Using our definitions of the time of last scattering surface and recombination from Sect. 3.1.1 and Sect. 3.1.2, we measured the logarithmic scale factor, redshift and cosmic time at these events. We present the results in Tab. 2 in addition to today's value of the freeze-out (FO) electron abundance and the sound horizon at decoupling. The number of significant figures is exaggerated to point out the small differences. The corresponding values resulting from the Saha equation is included in parentheses.

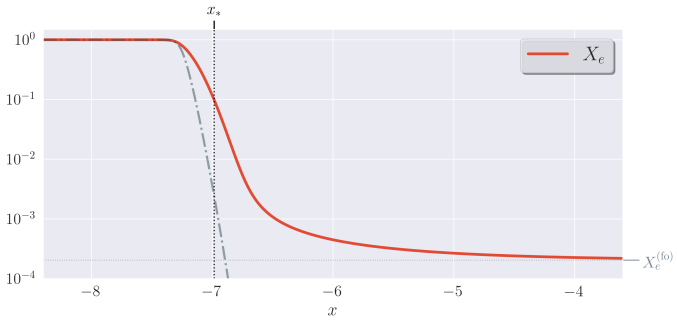

Fig. 6: The free electron fraction $X_e(x)$ resulting from the Saha and Peebles equations. The dash-dotted line represents the solution from the Saha equation only. Recombination onset is shown as the dotted vertical line.

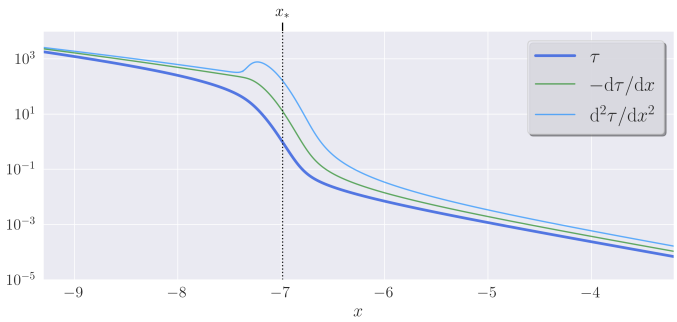

Fig. 7: The optical depth $\tau(x)$ and its derivatives $-\frac{\mathrm{d}\tau(x)}{\mathrm{d}x}$ and $\frac{\mathrm{d}^2\tau(x)}{\mathrm{d}x^2}$ as functions of logarithmic scale factor x. Recombination onset is shown as the dotted vertical line.

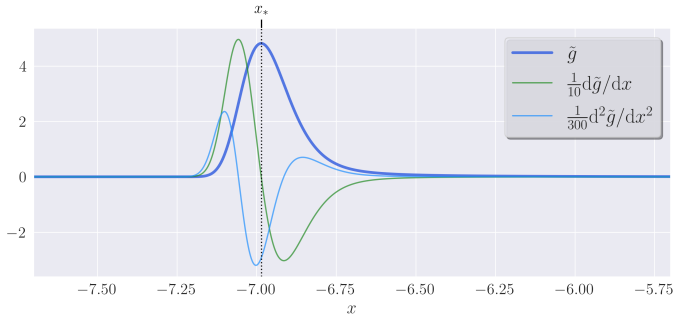

Fig. 8: The visibility function $\tilde{g}(x)$ and the shape of its derivatives $\frac{\mathrm{d}\tilde{g}(x)}{\mathrm{d}x}$ and $\frac{\mathrm{d}^2\tilde{g}(x)}{\mathrm{d}x^2}$ as functions of logarithmic scale factor x. Recombination onset is shown as the dotted vertical line.

3.4. Discussion

Overall, the results presented in the figures in Sect. 3.3 resemble those of a corresponding analysis by Callin (see 2006, Fig. 1, 2).

The graphs in Fig. 6 demonstrate the invalidity of the Saha solution for later times. The solid graph indicates a freeze-out electron fraction of order 10^{-4} – 10^{-3}, which we confirm in Tab. 2. We notice the decelerating decay rate at $x \sim -6.8$. Using our definitions of recombination onset and surface of last scattering, the Saha equation does not suffice for pinpointing the time for when these events occur. In this case, according to Tab. 2, the order of these events are reversed. However, these numbers rely on how we define the distinct events.

Table 2: The values of the logarithmic scale factor x, the redshift z and the cosmic time t corresponding to two events in the history of the universe. Values in parentheses are those we get with only the Saha equation.

	x	z	t
Recombination	−6.9854	1079.8	377.95 ka
	(−7.1404)	(1260.9)	(290.89 ka)
Last scattering surface	−6.9853	1079.7	378.04 ka
	(−7.1548)	(1279.3)	(283.81 ka)
FO free electron abundance:		$X_e^{(\mathrm{fo})} = 2.0261 \times 10^{-4}$	
Sound horizon at decoupling:		$r_s(x_*) = 145.30$ Mpc	

The optical depth in Fig. 7 tells us that the universe was very opaque before recombination, and that during the short period around recombination, the optical depth went from $\tau(-7.5) \sim 100$ to $\tau(-6.5) \sim 0.01$. After this epoch, the optical depth resumes its exponential decay. We see that $\tau(x_*) \approx 1$, as expected.

The visibility function is completely flat (zero) until just before $x = x_*$ where it rapidly increases to its maximum before an almost equally rapid decrease. However, there is a notable asymmetry in the probability function. The tail on the right side of the peak is longer than the one of the left. Together with Fig. 6, we take this to mean that, some time after recombination (see the slope in $X_e(x)$ at $x \sim -6.8$), there are still a significant portion of free electrons left to prevent photons to travel freely. In any case, the CMB photons last interacted with electrons between $x = -7.2$ and $x = -6$, most likely before $x = -6.7$.

Tab. 2 shows that recombination/photon decoupling occurred at redshift 1080 or 380 000 years after BB, consistent with concordance cosmology (e.g. Baumann (2015, Tab. 3.1)).[1] The free electron abundance has ceased to be only a single free electron for every 5000 hydrogen atoms, i.e. $X_e(x=0) = X_e^{(\mathrm{fo})} \approx 2 \times 10^{-4}$. Sound waves managed to travel maximum 145 Mpc before frozen in.

4. Conclusion

References

Baumann, D. 2015, Cosmology: Part III Mathematical Tripos
Betoule, M., Kessler, R., Guy, J., et al. 2014, A&A, 568, A22
Callin, P. 2006, arXiv e-prints, astro
Dodelson, S. & Schmidt, F. 2021, Modern Cosmology, 2nd edn.
Ma, C.-P. & Bertschinger, E. 1995, ApJ, 455, 7
Peebles, P. J. E. 1968, ApJ, 153, 1
Planck Collaboration, Aghanim, N., Akrami, Y., et al. 2021, A&A, 652, C4

[1] There is an implicit wiggle room when we say "consistent" in this context, as there are several ways of defining recombination onset and the last scattering surface.

Appendix A: Conformal Hubble parameter

Revisit the general form of the first Friedmann equation from Sect. 2.1.2, i.e.

$$\mathcal{H}(x) = H_0 \sqrt{\sum_s \Omega_{s0} e^{-(1+3w_s)x}}, \tag{A.1}$$

where sum over s is a sum over the constituents in the universe ($s \in \{\mathrm{m}, \mathrm{r}, \Lambda, \mathrm{K}\}$) and w_s represents the species' equation of state parameter. As a shorthand notation, we introduce $\Xi_m = \Xi_m(x)$ given by

$$\Xi_m(x) \equiv \sum_s (-1)^m (1+3w_s)^m \Omega_{s0} e^{-(1+3w_s)x}; \quad m \in \mathbb{N}, \tag{A.2}$$

s.t. $\mathrm{d}^n X_m/\mathrm{d}x^n = \Xi_{m+n}$. Now $\mathcal{H} = H_0\sqrt{\Xi_0}$ and its first derivative becomes

$$\frac{\mathrm{d}\mathcal{H}}{\mathrm{d}x} = H_0 \frac{\Xi_1}{2\sqrt{\Xi_0}}. \tag{A.3}$$

The second derivative is obtained through the quotient rule, i.e.

$$\begin{aligned}\frac{\mathrm{d}^2\mathcal{H}}{\mathrm{d}x^2} &= \frac{H_0}{2} \frac{\Xi_2\sqrt{\Xi_0} - \Xi_1 \frac{\Xi_1}{2\sqrt{\Xi_0}}}{\Xi_0} \\ &= H_0 \frac{\Xi_1}{2\sqrt{\Xi_0}} \left(\frac{\Xi_2}{\Xi_1} - \frac{\Xi_1}{2\Xi_0} \right).\end{aligned} \tag{A.4}$$

Now that we have these expressions, let us look at some special cases. Assume that the universe only consists of the substance s. Then

$$\Xi_m = (-1)^m (1+3w_s)^m \Omega_{s0} e^{-(1+3w_s)x}. \tag{A.5}$$

We obtain the following:

$$\frac{1}{\mathcal{H}}\frac{\mathrm{d}\mathcal{H}}{\mathrm{d}x} = \frac{\Xi_1}{2\Xi_0} = -\frac{1}{2}(1+3w_s) \tag{A.6a}$$

$$\frac{1}{\mathcal{H}}\frac{\mathrm{d}^2\mathcal{H}}{\mathrm{d}x^2} = \frac{\Xi_1}{2\Xi_0}\left(\frac{\Xi_2}{\Xi_1} - \frac{\Xi_1}{2\Xi_0}\right) = +\frac{3}{4}(1+3w_s)^2 \tag{A.6b}$$

As for the conformal time, we get an expression that is ill-defined for some cases:

$$\begin{aligned}\frac{\eta\mathcal{H}}{c} &= \mathcal{H} \int_{-\infty}^{x} \mathrm{d}x' \, \frac{1}{\mathcal{H}} \\ &= e^{\frac{x}{2}(1+3w_s)} \int_{-\infty}^{x} \mathrm{d}x' \, e^{-\frac{x'}{2}(1+3w_s)} \\ &= \begin{cases} \frac{2}{1+3w_s} & w_s > 1/3 \\ \infty & w_s \leq -1/3 \end{cases}\end{aligned} \tag{A.7}$$

We have gathered a set of analytical predictions for different eras in the history of the universe. The detailed result is presented in Tab. A.1. Note, however, that to compare this last expression to the numerical result does not actually make sense for later times as $\eta(x)$ depends on the historic composition as well.

Table A.1: Analytical predictions for single-substance universes.

	w_s	$\mathcal{H}/H_0$	$\frac{1}{\mathcal{H}}\frac{\mathrm{d}\mathcal{H}}{\mathrm{d}x}$	$\frac{1}{\mathcal{H}}\frac{\mathrm{d}^2\mathcal{H}}{\mathrm{d}x^2}$	$\frac{\eta\mathcal{H}}{c}$
Radiation-dominated	$1/3$	$\sqrt{\Omega_{\mathrm{r}0}}e^{-x}$	-1	1	1
Matter-dominated	0	$\sqrt{\Omega_{\mathrm{m}0}}e^{-1/2x}$	$-1/2$	$1/4$	2
DE-dominated	-1	$\sqrt{\Omega_{\Lambda 0}}e^{x}$	1	1	∞